Aerosol Science and Technology

ISSN: 0278-6826 (Print) 1521-7388 (Online) Journal homepage: https://www.tandfonline.com/loi/uast20

The versatile size analyzing nuclei counter (vSANC)

Tamara Pinterich, Aron Vrtala, Merzuk Kaltak, Juha Kangasluoma, Katrianne Lehtipalo, Tuukka Petäjä, Paul M. Winkler, Markku Kulmala & Paul E. Wagner

To cite this article: Tamara Pinterich, Aron Vrtala, Merzuk Kaltak, Juha Kangasluoma, Katrianne Lehtipalo, Tuukka Petäjä, Paul M. Winkler, Markku Kulmala & Paul E. Wagner (2016) The versatile size analyzing nuclei counter (vSANC), Aerosol Science and Technology, 50:9, 947-958, DOI: 10.1080/02786826.2016.1210783

To link to this article: https://doi.org/10.1080/02786826.2016.1210783

Published online: 08 Jul 2016.

AEROSOL SCIENCE AND TECHNOLOGY
2016, VOL. 50, NO. 9, 947–958
http://dx.doi.org/10.1080/02786826.2016.1210783

The versatile size analyzing nuclei counter (vSANC)

Tamara Pinterich[a,*], Aron Vrtala[a], Merzuk Kaltak[a,**], Juha Kangasluoma[b], Katrianne Lehtipalo[b,***], Tuukka Petäjä[b], Paul M. Winkler[a], Markku Kulmala[b], and Paul E. Wagner[a]

[a]Faculty of Physics, University of Vienna, Vienna, Austria; [b]Department of Physics, University of Helsinki, Helsinki, Finland

ABSTRACT

We present a new field-deployable expansion chamber condensation particle counter—the versatile size analyzing nuclei counter (vSANC). The measuring principle, which was adopted from the classical SANC, was optimized regarding ranges of operating temperatures (−20°C to +40°C), inlet gas pressures (0.2–1.2 bar), inlet flow rates (1.6–9 l/min) and condensing liquids (alcohols, alcanes, water, etc.), all of which make vSANC applicable to a wide variety of environments. Precision determination of vapor supersaturation ratios allows estimating neutral cluster sizes without prior electrical-mobility based classification of the sample. Additionally, absolute number concentrations ranging from 10^2 to $10^7 cm^{-3}$ can be measured without referring to external calibration standards. This enables size-resolved number concentration measurements of nanoparticles. Laboratory studies using n-propanol as condensing liquid demonstrated that charged $(NH_4)_2SO_4$ and WO_x particles as small as 1.5 nm can be counted with an efficiency of 10%. Furthermore, we observed an increase in counting efficiency of charged WO_x particles by about 50% when lowering vSANC's chamber and saturator temperatures from 23°C and 25°C to 13°C and 15°C, respectively. During spring 2014, the vSANC was operated at the SMEAR II station in Finland where the formation and growth of atmospheric clusters was investigated. Atmospheric new particle formation (NPF) was observed only when vSANC's operating temperatures (13°C and 15°C) were close to the ambient air temperature (about 5°C–15°C). Diurnal concentration evolution measured with the vSANC was compared with data from a differential mobility particle sizer (DMPS) and a nano-condensation nucleus counter (nCNC, Airmodus A11). vSANC detected the NPF signal 2–3 h before the DMPS in agreement with the nCNC; however, a continuously present pool of highly concentrated neutral clusters in the sub-3 nm diameter range could not be confirmed during these measurements.

ARTICLE HISTORY
Received 21 March 2016
Accepted 26 June 2016

EDITOR
Susanne Hering

1. Introduction

Atmospheric nanoparticle formation by gas-to-particle conversion is frequently observed in field measurements and is thought to be one major source controlling aerosol number distributions on the global scale (Kulmala et al. 2004). Both model studies and observations have shown that these nanoparticles can grow to sizes where they act as cloud condensation nuclei (Kalivitis et al. 2015; Sihto et al. 2011; Merikanto et al. 2009; Spracklen et al. 2008). Thereby they contribute to the indirect radiative forcing, which ultimately affects climate. Regarding the initial steps of atmospheric new particle formation (NPF), Kulmala et al. (2013) recently presented an observation-based framework, which confirmed that for boreal forest sites the formation of nanoparticles in the atmosphere is essentially a two-step process dominated by neutral pathways. In the first step, clusters between 1.2 and 1.7 nm grow predominantly by sulfuric acid and are stabilized by ammonia and amines, whereas in the second step the growth of clusters bigger than 1.7 nm is enhanced by oxidized organic vapors. However, the mechanisms responsible for these processes remain poorly understood. Part of the difficulties is related to certain fundamental limits in the detection of nanoparticles by available instrumentation (McMurry 2000a). So far, only condensation particle counters (CPCs) are able to measure neutral gas-borne particles that are too small for optical detection methods.

The history of CPCs spans more than a century and extends back to the work of Aitken (1888) (McMurry

CONTACT Tamara Pinterich tpinterich@bnl.gov Brookhaven National Laboratory, Environmental and Climate Sciences Department, Bldg. 815, P.O. Box 5000, Upton, NY 11973-5000, USA.
*Current affiliation: Environmental and Climate Sciences Department, Brookhaven National Laboratory, Upton, New York, USA.
**Current affiliation: Physics and Astronomy Department, Stony Brook University, New York, USA.
***Current affiliation: Paul Scherrer Institute, Villigen, PSI, Switzerland.

2000b). However, only recently CPCs capable of detecting particles down to 3 nm in diameter and below have become available. Substantial progress in instrumentation has been achieved by means of various sophisticated approaches. For example the ultrafine laminar flow condensation nucleus counter (UCPC, TSI Model 3025) developed by Stolzenburg and McMurry (1991) minimizes sampling losses of small particles by using an aerosol sheathing technique. A mixing-type CPC developed by Okuyama et al. (1984) showed the ability of detecting charged particles down to 1.5 nm (Seto et al. 1997). Gamero-Castaño and Fernandez de la Mora (2000, 2002) have introduced a reheater to Okuyama's original design to overcome homogeneous nucleation pushing the lower size limit even further. Hering et al. (2005) introduced water as working fluid for a laminar flow CPC (TSI Model 3785), which depending on the chemical composition of condensation nuclei showed similar counting efficiency curves as the UCPC. Using an expansion chamber CPC (SANC, Wagner et al. 2003) Winkler et al. (2008a) showed that with n-propanol as working fluid neutral particles below 2 nm could be detected via condensational growth techniques. Sipilä et al. (2008) demonstrated, that CPCs can be used for detecting atmospheric sub-3 nm particles and clusters, and later introduced a pulse-height CPC for quantifying the sub-3 nm concentrations (Sipilä et al. 2009). Iida et al. (2009) used a UCPC with diethylene glycol (DEG) as working fluid, and succeeded in activating particles below 2 nm. Vanhanen et al. (2011) developed a field-applicable Particle Size Magnifier (PSM) (Airmodus Model A09) using DEG as working fluid that showed high detection efficiencies of sub-2 nm particles. Kuang et al. (2012) demonstrated that by increasing saturator temperature and condenser flow rate the UCPC's counting efficiency of particles down to about 1 nm could be significantly improved.

The objective of this study is to present a recently developed expansion-type CPC—the versatile Size Analyzing Nuclei Counter (vSANC)—and its application to atmospheric aerosol studies. The measuring principle of vSANC, which was adopted from the classical SANC, features high flexibility regarding operating temperatures, total gas pressures, aerosol intake flow rates and working fluids. Compared to SANC, vSANC is not restricted to laboratory experiments, has a lowest detectable concentration limit of 10^2 cm^{-3}, and more than five times higher counting statistics. This makes vSANC applicable to a wide range of environments (e.g., regarding temperature, altitude, and pollution level), without losing SANC's high measurement precision. In contrast to other field applicable CPCs, the vSANC's ability of determining vapor supersaturation ratios allows sizing of neutral nanoparticles without prior electrical mobility classification. Moreover, vSANC utilizes an indirect optical measurement techniques to obtain absolute particle number concentrations, which results in a higher upper detectable number concentration limit, that is, about 10^7 cm^{-3}, compared to other CPCs measuring in single-particle-counting mode.

The vSANC was operated at Station for Measuring Ecosystem—Atmosphere Relations (SMEAR II; Hari and Kulmala 2005) station during Biogenic Aerosols—Effects on Clouds and Climate (BAECC) study (Petäjä et al. 2016). Laboratory studies with vSANC showed that $(NH_4)_2SO_4$ and WO_x clusters down to about 1 nm can be activated. Thus vSANC is a promising instrument that might help solving the aerosol nucleation puzzle (Andreae 2013) by providing size resolved absolute number concentration measurement of neutral sub-3 nm particles in a concentration range that spans about six orders of magnitude.

2. Instrument description

2.1. Measuring principle

The measuring principle of the vSANC is based on the activation of particles by heterogeneous nucleation of supersaturated vapor. Thereby particles grow into sizes where they can be detected optically. In the present study, we used n-propanol (Merck, Purity > 99.95%) as condensing liquid. Particle number concentrations N_c and droplet growth data $d_p(t)$ can be determined applying the multi-angle Constant Angle Mie Scattering (mCAMS) method (detailed information on the mCAMS method will be provided in another article, which is currently in preparation). The mCAMS method is a further development of the CAMS method introduced by Wagner (1985). Droplets growing inside the measurement chamber are illuminated by a polarized laser beam ($\lambda = 488$ nm, JSDU Type FCD488). The light flux $\Phi_s(\theta, t)$, scattered by these droplets, is monitored at five different scattering angles, $\theta = 10°$, 15°, 20°, 25°, and 30°, on both sides of the incident laser beam axis simultaneously.

Additionally the total light flux $\Phi_t(t)$ transmitted through the expansion chamber is measured. Moreover, light attenuation by particles already visible before expansion, can be accounted for by observing a reference baseline provided by an additional photo detector monitoring the incident laser light flux using a beam splitter. This allows compensating for possible intensity changes of the incident laser beam, for example, due to light scattering of bigger particles before expansion. A schematic diagram of the scattering geometry is shown in Figure 1. Scattered and transmitted light fluxes are measured

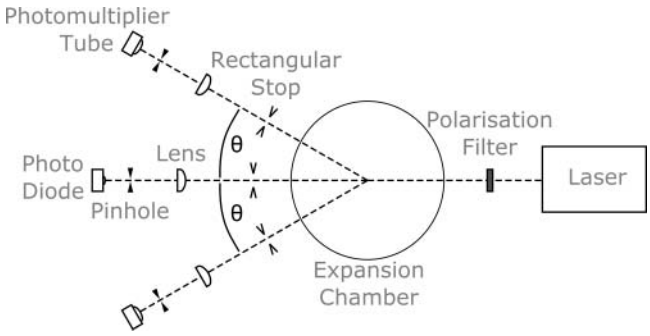

Figure 1. Schematic diagram of the mCAMS method.

applying lens-pinhole detector systems. Thereby light scattered in forward direction can almost completely be eliminated when measuring $\Phi_t(t)$. For measurements of $\Phi_s(\theta, t)$, the use of a lens-pinhole system allows to increase the detected light flux, while at the same time the influence of light scattered in directions different from θ on positions of experimental Mie extrema can be kept negligibly small.

By normalizing experimental scattered light fluxes with respect to light attenuation, i.e., the ratio of Φ_t during droplet growth to Φ_t before expansion, the influence of extinction on height and position of experimental extrema (Figure 2) can be eliminated. Normalized experimental scattered light flux vs. time curves $\Phi_s(t)$ show series of extrema in excellent agreement with theoretical scattered light flux vs. droplet size curves $\Phi_s(d_p)$ (Figure 3).

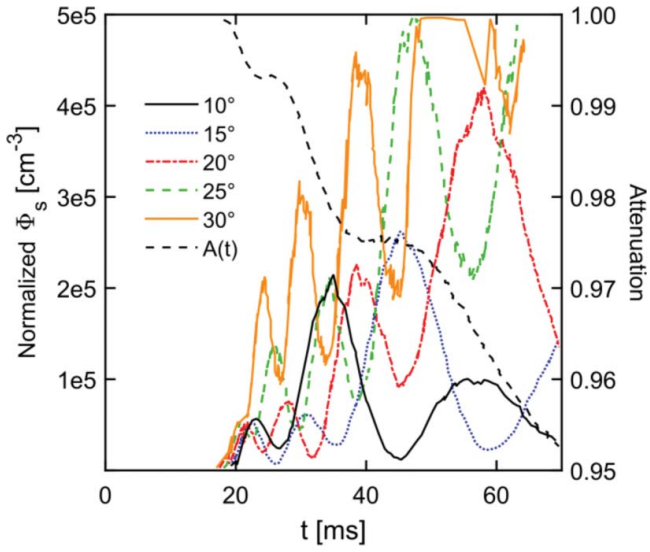

Figure 2. Typical set of normalized scattered light fluxes Φ_s and light attenuation A, that is, the ratio of total light flux $\Phi_t(t)$ measured during expansion to Φ_t measured before expansion. Φ_s is simultaneously monitored at light scattering angles $\theta = 10°$, 15°, 20°, 25°, and 30°, which are given with different hues (colors). Light fluxes were measured during growth of ambient aerosol particles in n-propanol vapor. The droplet number concentration was about 5×10^2 cm^{-3}.

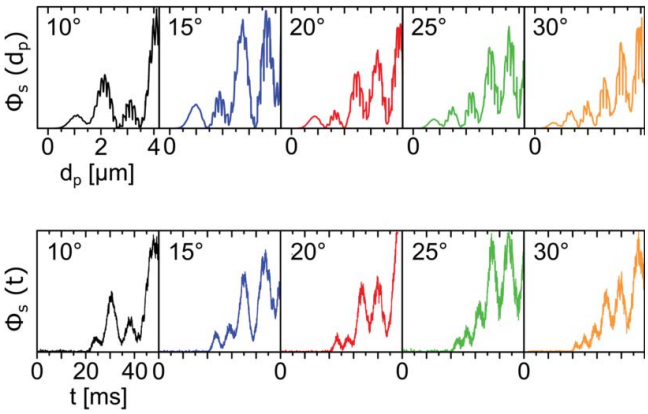

Figure 3. Theoretical (top) and experimental (bottom) scattered light fluxes for five different light scattering angles θ.

This allows the establishment of a one-to-one correspondence between experimental and theoretical maxima and minima. Comparing positions of experimental to corresponding theoretical extrema yields droplet diameters at specific times during growth (Figure 4), which enables precision determination of vapor supersaturation ratios as will be shown later.

In the absence of multiple scattering, dependent scattering and polarization field interactions, the height of normalized scattered light fluxes is proportional to the number concentration of particles inside the chamber (Wagner 1985). In the present study, number concentrations were calculated from the height of the first global Mie maximum. To this end, photomultiplier tubes

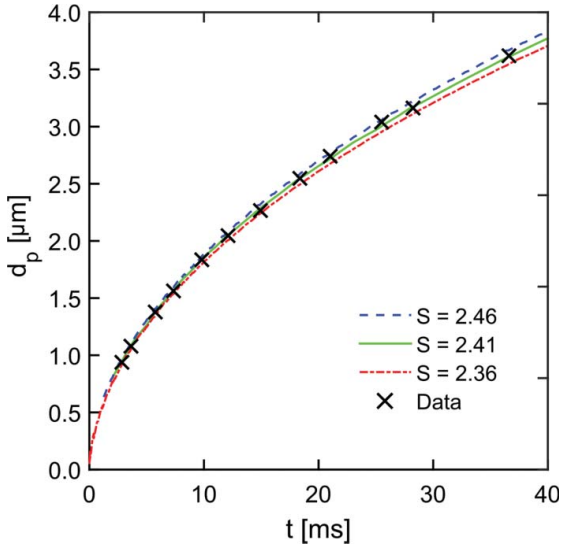

Figure 4. Experimental droplet growth data (crosses) and theoretical droplet growth curves (lines) calculated for three different vapor supersaturation ratios S. The absolute pressure before expansion was 985.5 mbar, the expansion ratio 1.37, the temperature after expansion 2.61°C and the droplet number concentration after expansion 5×10^4 cm^{-3}.

measuring $\Phi_s(\theta, t)$ were calibrated using the extinction method (Szymanski and Wagner 1990). This yields five absolute values for N_c per expansion experiment without referring to empirical calibrations by external reference standards.

Measurement of $\Phi_s(t)$ at multiple angles and the illumination of droplets with blue instead of red laser light increases the number of independent (d_p, t) pairs compared to classical SANC measurements. These additional data are particularly beneficial both in the high droplet concentration regime, where growth may suffer from vapor depletion, as well as at low concentrations, where experimental Mie extrema may not be well pronounced. Hence the mCAMS method enables determination of number concentrations and droplet growth curves in a wider concentration range, that is, 10^2 cm^{-3} to 10^7 cm^{-3}.

It should be noted, that in case homogeneous nucleation occurs in the expansion chamber in addition to heterogeneous nucleation, time resolved light flux measurements enable distinguishing the signals of heterogeneously formed droplets from homogeneously formed ones (Winkler et al. 2008b). This distinction is possible because signals from heterogeneously formed droplets will always appear at lower supersaturation, which will be reached earlier during the expansion process (Figure 5).

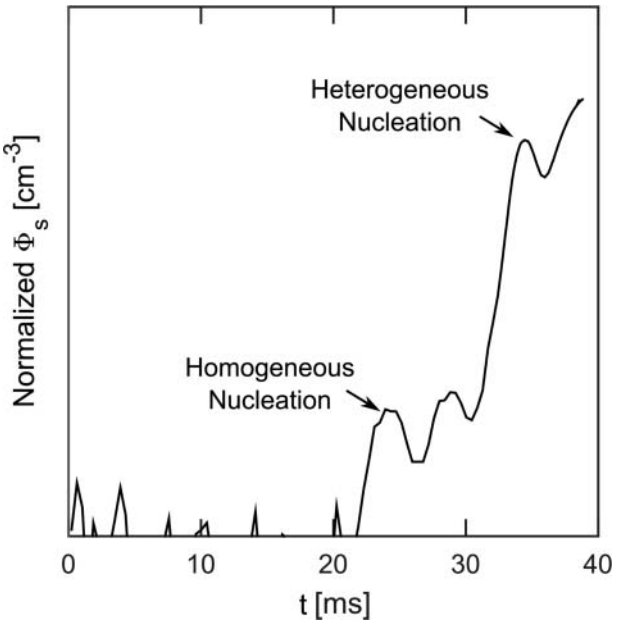

Figure 5. Normalized scattered light flux measured at 15° forward scattering direction. Note the *y*-axis is scaled logarithmically. The first Mie maximum appearing at around 25 ms represents heterogeneously formed droplets ($N_c \sim 10^3$ cm^{-3}). The third maximum (t ~ 35 ms) corresponds to homogeneously formed droplets ($N_c \sim 10^5$ cm^{-3}).

This feature of vSANC becomes particularly useful, when sub-2 nm particles are to be measured.

Besides light flux measurements, the temperature of the particle-vapor-gas mixture before expansion T_i, the total gas pressure p_i before expansion, the total pressure change during expansion Δp and the saturator temperature T_{sat} are monitored. Knowing vapor saturation ratio S_{sat} at the exit of the saturator and vapor supersaturation S_0 at the end of the expansion can be calculated. Provided that the expansion process is dry adiabatic and quasi-static S_0 can be expressed as

$$S_0 = \frac{S_{sat} \cdot p_s(T_{sat})}{\beta \cdot p_s(T_0)}, \quad [1]$$

where β is the expansion ratio, i.e. the ratio of p_i to $p_i - \Delta p$. The temperature T_0 at the end of expansion is given by Poisson's law

$$T_0 = T_i \beta^{\frac{1-\kappa}{\kappa}} \quad [2]$$

with adiabatic index κ given by the Richarz formula (Richarz 1906). Since droplet growth strongly depends on S_0, experimentally determined $d_p(t)$ curves can be used to verify S_0. On the other hand, if S_{sat} is unknown, S_0 can be determined by comparing experimental $d_p(t)$ data with theoretical $d_p(t)$ curves (Vesala et al. 1997; Wagner 1982), which depend on parameters such as diffusion and accommodation coefficients.

Both N_c and S_0 are key requisite to perform quantitative nucleation studies. To this end, S_0 is stepwise increased until all particles in the expansion chamber are activated. This results in experimental heterogeneous nucleation probability curves $P(S_0)$, which give the fraction of activated particles as a function of S_0. From experimental $P(S_0)$ curves, the onset saturation ratio S_{onset}, which is defined as the vapor saturation ratio where 50% of all particles are activated, can be determined. S_{onset}, in turn, can be used to estimate the diameter of seed particles that can be activated according to Fletcher theory (Fletcher 1958; Vehkamäki et al. 2007; Winkler et al. 2012), from now on referred to as Fletcher diameter.

2.2. Instrument design

The vSANC is comprised of a cylindrical stainless steel expansion chamber (diameter ~ 4 cm), a 30-cm-long diffusion-type saturator, a subpressure vessel *R*, vacuum pumps, pressure and temperature sensors, 2–2 way valves and connecting tubing. The volume of the expansion chamber is about four times smaller than the volume of *R*, which makes changes in total gas pressure

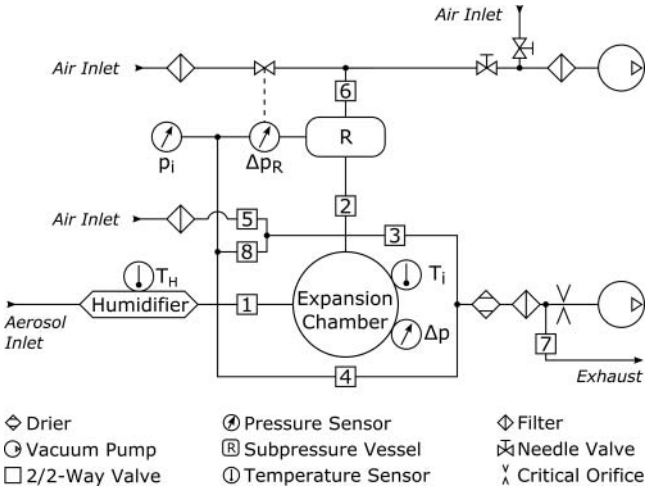

Figure 6. Flow diagram of vSANC.

after expansion practically negligible. Thus, the expansion chamber is pressure defined. A schematic diagram of the instrument setup is shown in Figure 6. The aerosol inlet line consisting of saturator, inlet valve 1 and stainless steel tubing is about 70 cm. Not shown in Figure 6 is the integrated optics assembly (IOA), which is directly attached to the expansion chamber. The IOA consists of two identical glassfibre-reinforced plastic (PEEK) plates equipped with optical elements, such as lenses, pinholes, and photosensors. The properties of PEEK enable light flux measurements at chamber temperatures ranging from −20°C to + 40°C.

A LabView-based program controls and automates the measurement process. To enable good reproducibility the timing of experiment is defined by an automated valve cycle. At the beginning of the cycle, humidified aerosol is flushed through the expansion chamber, while a preset vacuum Δp_R is generated in R (valves 1, 3, and 6 open). A vacuum pump along with a critical orifice is used to maintain a constant aerosol flow through the chamber, that is, active sampling mode. However, it is also possible to operate the vSANC in passive sampling mode by opening valve 7 and stopping the vacuum pump. In that case aerosol flow is externally controlled. After sufficient flushing, aerosol in the expansion chamber can equilibrate with its surrounding by closing valves 1 and 3. In the meanwhile aerosol entering the instrument flows toward the exhaust via a bypass line (valve 4 open) enabling continuous aerosol flow. Before the cycle switches to expansion, valve 6 is closed. Then expansion chamber and R are connected by opening expansion valve 2. About 500 ms before and during expansion system temperatures T_{sat} and T_i, system pressures Δp, Δp_R, and p_i, and light fluxes Φ_s and Φ_t are recorded. PID controlled system temperatures are monitored utilizing PT100 sensors connected to a digital multimeter (Keithley 2700). Rapid changes in Δp during expansion are measured using a piezo-sensor (Kistler 7031). Δp_R and p_i are monitored with pressure transducers (MKS 628A and 220D). Scattered light fluxes are measured using photomultiplier tubes (Hamamatsu H7827_002) while transmitted and incident light fluxes are measured with photo diodes (Centronic OSD35-5T). After completed data acquisition valve 2 is closed. Pressure compensation between vacuum in the expansion chamber and ambient air pressure is achieved by briefly opening valve 5 before returning to flushing position (valve 1, 3, and 6 open). In general vSANC can be operated at system pressures ranging from 0.2 to 1.2 bar. It is also possible to run measurements at system pressures different from ambient air pressure by opening valve 8 instead of 5.

A complete measuring sequence takes about 40 s providing the lower time resolution for determination of N_c and S_0. It is limited by the equilibration rate of the aerosol inside the expansion chamber and the comparatively slow pressure control unit (MKS 250E) regulating Δp_R.

2.3. Laboratory characterization setup

The vSANC was characterized using monodisperse seed particles of different chemical composition, such as ammonium sulfate ($(NH_4)_2SO_4$), tungsten oxide (WO_x), silver (Ag), and sodium chloride (NaCl), suspended in dried and filtered air. A schematic diagram of the experimental setup is shown in Figure 7. NaCl and $(NH_4)_2SO_4$ particles ranging from about 1 to 7 nm in diameter were generated by evaporation-condensation growth using a tube furnace (Kangasluoma et al. 2013; Scheibel and Porstendörfer 1983). Sub-3 nm WO_x particles were generated using a Grimm WO_x generator (Grimm Aersosoltechnik, Model 7.860; Steiner 2006). Polydisperse particles generated by either of these two methods were subsequently charged bipolarly in an Am241 charger (Reischl et al. 1983) and classified in a high-resolution differential mobility analyzer (DMA). Experiments with $(NH_4)_2SO_4$ particles were conducted at the University of Helsinki, where we used a Herrmann-type

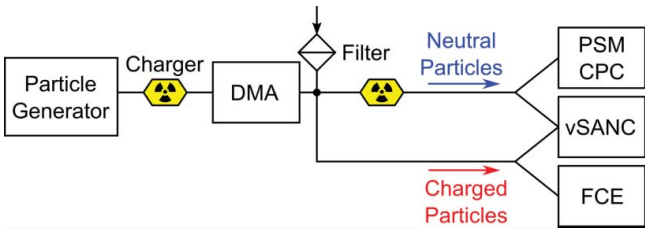

Figure 7. A schematic diagram of the experimental setup for instrument characterization.

high-resolution DMA (Kangasluoma et al. 2016). NaCl, Ag, and WO_x particles were classified with a Vienna type high-resolution DMA (Reischl et al. 1997) at the University of Vienna. Thereby a monodispersed particle number size distribution with a geometrical mean standard deviation of typically 1.06 was obtained. After classification the aerosol was split into two flows, one directed to a reference particle counter and the other to vSANC. In case of charged particles, a Faraday cup electrometer (FCE, TSI Model 3068b) was used as reference instrument (Liu and Kim 1977). Particles neutralized downstream of the DMA were reference-counted with a mixing-type particle size magnifier (PSM; Airmodus Model A10) capable of activating particles below 3 nm, in combination with a laminar flow CPC (TSI Model 3776/Vienna calibration or Airmodus Model A20/Helsinki calibration) to enlarge activated particles to optically detectable sizes (Okuyama et al. 1984). From now on this reference counting setup will be referred to as nCNC (nano condensation nucleus counter).

In the present study, vSANC was always operated in active sampling mode at ambient air pressure. The size of the critical orifice regulating the aerosol flow was chosen to maximize the number of particles entering the measuring chamber. For laboratory measurements aerosol intake flow rates typically ranged from 1.6 to 9 l/min. For field studies, where sample dilution was not of concern, the inlet flow rate was always 9 l/min. Two different temperature settings were used to investigate the temperature dependence of vSANC's counting efficiency. In the following high temperature settings refer to chamber and saturator temperatures of 25°C and 23°C, respectively. Low temperature settings correspond to T_i and T_{sat} of 15°C and 13°C, respectively. Because of its ability to nucleate on particles as small as 1 nm (Winkler et al. 2008a) n-propanol was used as working fluid for all experiments presented here.

Size-dependent vSANC counting efficiencies were investigated as a function of particle composition, system temperatures, and charging state (positively charged or neutral). To this end, particle number concentrations measured by vSANC, N_{vSANC}, were compared to those simultaneously measured by FCE or nCNC. To ensure that all particles reaching the expansion chamber were counted, the vapor supersaturation S_0 was increased up to the limit of homogeneous nucleation until $N_{vSANC}(S_0)$ reached a plateau.

2.4. Ancillary field measurements

In the field, our goal was to investigate the formation and growth of atmospheric clusters starting from smallest detectable sizes. To this end, the vSANC was operated in scanning mode sampling ambient aerosol without prior electrical mobility classification at an intake flowrate of 9 l/min using n-propanol as working fluid. Thereby size-dependent particle activation is achieved by altering the expansion ratio β among three different values. Accordingly, concentration measurements in three different particle diameter bins were performed sequentially, one full measuring sequence taking about 6 min. The margins of different size bins were approximated using Fletcher theory and experimentally determined S_0.

At the highest S_0 where homogeneous nucleation was observed basically all clusters capable of acting as condensation nuclei for n-propanol vapor can be considered activated.

To check the stable performance of vSANC, zero measurements were performed in the morning and evening of each measurement day. To this end, a HEPA filter was installed at the instrument inlet and the onset of homogeneous nucleation was investigated by stepwise increasing the pressure drop in the expansion chamber.

3. Results and discussion

3.1. Counting efficiency

In general, the size-dependent counting efficiency $\eta(d_{seed})$ of a CPC can be factored into the product (Stolzenburg and McMurry 1991)

$$\eta(d_{seed}) = \eta_{sam}(d_{seed}) \cdot \eta_{act}(d_{seed}) \cdot \eta_{det}(d_{seed}) \qquad [3]$$

where η_{sam}, η_{act}, and η_{det} are sampling, activation and detection efficiencies, respectively. The sampling efficiency η_{sam} is defined as the ratio of particle concentration of the aerosol exiting the sampling line to that entering it. The activation efficiency η_{act} is defined as the fraction of particles activated by means of heterogeneous nucleation. The detection efficiency, η_{det}, is the fraction of activated particles, that grow large enough to be detected optically.

In case of vSANC counting efficiencies mainly depend on sampling efficiencies η_{sam}, which are determined by particle losses along the sampling line and during delay inside the expansion chamber. Once sufficiently high vapor supersaturation is achieved after adiabatic expansion experimental heterogeneous nucleation probabilities allow to verify that nearly all particles are activated ($P(S_0) \approx 1$). In the present study particle number concentrations, N_{vSANC}, used to calculate vSANC counting efficiencies always refer to heterogeneous nucleation probabilities close to 100% thus $\eta_{act} \approx 1$. Regarding the detection efficiency of vSANC, optical detection applying the mCAMS method indicates, that the droplets growing

into optically detectable sizes are sufficiently monodisperse. Thus, either all droplets grow large enough to be detected or none of them. Hence, for particle number concentrations ranging from 5×10^2 to 10^7 cm^{-3}, the detection efficiency is close to 1, as well.

In contrast to vSANC, counting efficiencies η of CPCs are mainly determined by activation efficiencies η_{act}. Activation efficiencies, in turn, tend to have stronger size dependence than sampling efficiencies η_{sam}. Thus, size-dependent counting efficiency curves $\eta(d_{seed})$ of laminar flow or mixing-type CPCs are steeper than vSANC's counting efficiency curve. Figure 8 shows $\eta(d_{seed})$ of various CPCs including vSANC for positively charged ammonium sulfate particles.

The cut-off diameter, d_{50}, of vSANC is about 4.3 nm, which is clearly larger than those of a laminar-flow CPC (modified TSI Model 3025, green diamonds) or the nCNC (Airmodus Model A11, red diamonds). However, the comparatively weak size dependence of vSANC counting efficiencies yields similar d_{10}, that is, seed particle diameters corresponding to 10% counting efficiency, of about 1.5 nm. Above about 1.8 nm vSANC detects a smaller fraction compared to both CPCs. This reflects the fact that vSANC counting efficiencies are mainly determined by sampling efficiencies whereas counting efficiencies of laminar-flow or mixing-type CPCs usually depend on activation efficiencies, and in general η_{sam} has weaker size dependence than η_{act}, as mentioned earlier.

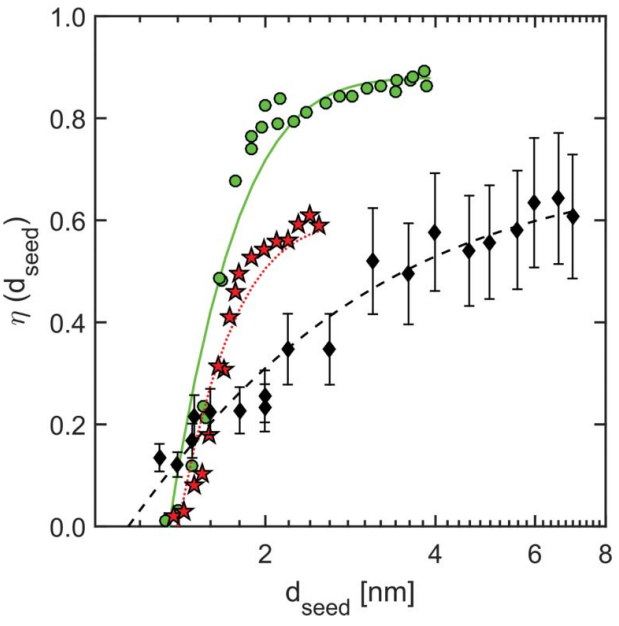

Figure 8. Size dependent CPC counting efficiencies of positively charged ammonium sulfate particles. Diamonds (black) refer to vSANC counting efficiency data. Circles (green) and stars (red) are *activation* efficiencies of an ultrafine CPC (modified TSI Model 3025; Iida et al. 2009) and a nCNC (Airmodus Model A11), respectively, both using diethylene glycol as working fluid.

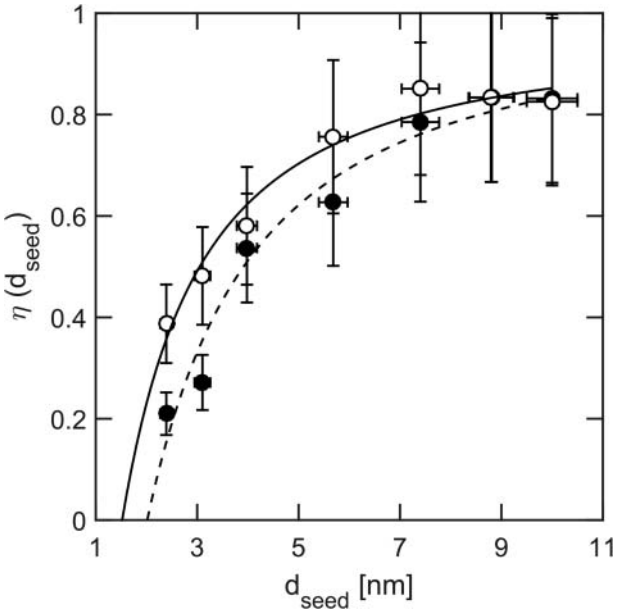

Figure 9. vSANC counting efficiency as a function of seed particle diameter for charged (solid circles) and neutral (open circles) silver particles.

High inlet losses are partly due to the fact that the particles entering vSANC are not activated until the moment of expansion, which is a fundamental difference between expansion type and laminar flow or mixing-type CPCs. Additionally, the plastic sleeve of the inlet valve negatively affects the penetration of both charged as well as polar particles. It is, therefore, planned to replace the current inlet valve by a stainless steel ball valve.

Figure 9 shows vSANC counting efficiencies of neutral and charged silver particles. It can be seen that the smaller the particles, the larger the difference in the counting efficiencies between charged and neutral seed particles becomes. For seed particles below 4 nm in diameter, the penetration of neutral particles is about 50% higher than the one of charged seeds. This unexpected behavior can most probably be explained by a 10-cm-long plastic pinch valve installed along the inlet, which acts as ion trap.

Counting efficiencies of positively charged tungsten oxide particles are shown in Figure 10. $\eta(d_{seed})$ increased by about 50%, when expansion chamber and saturator temperatures were decreased from 25°C and 23°C, to 15°C and 13°C, respectively. The positive effect of low temperature settings was also observed during field measurements and might be related to the temperature dependence of heterogeneous nucleation reported by Kupc et al. (2013) and Schobesberger et al. (2010).

At low temperature settings, the counting efficiency of positively charged tungsten oxide particles with diameters between 1.3 and 1.6 nm range from 8 to 18%, with d_{10} being about 1.5 nm.

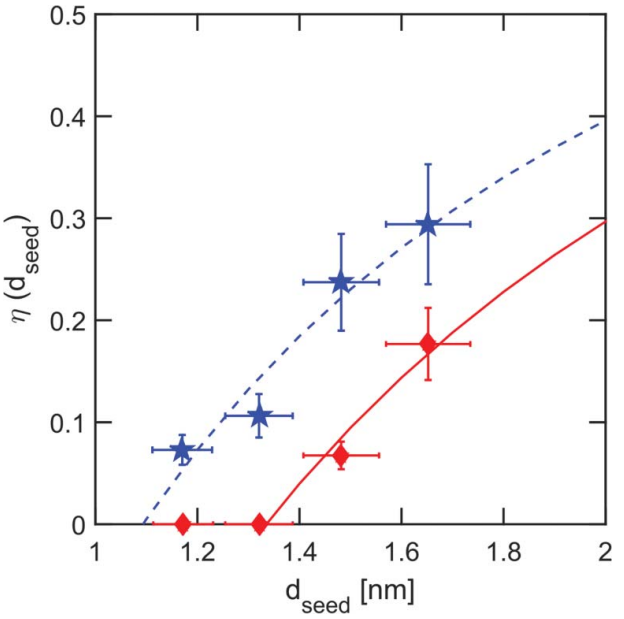

Figure 10. vSANC counting efficiency of positively charged tungsten oxide particles. Stars (blue) and diamonds (red) refer to expansion chamber temperatures of 15°C and 25°C, respectively.

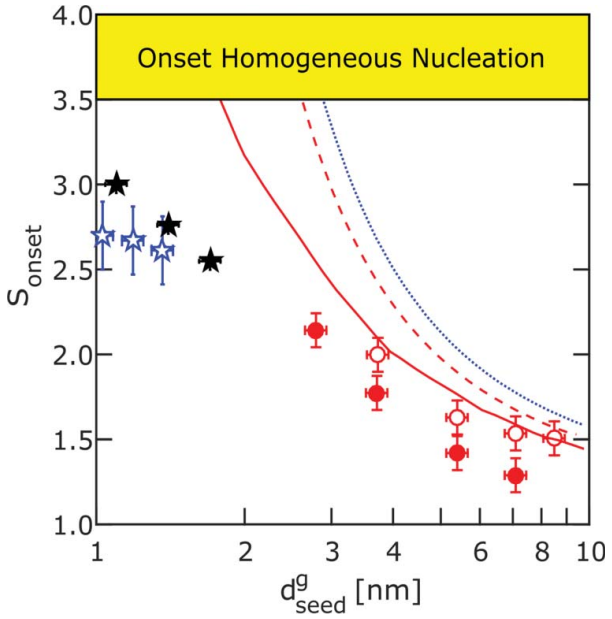

Figure 11. N-propanol onset saturation ratio S_{onset} as a function of geometric seed particle diameter d^g_{seed}. Stars and circles represent experimentally determined onset saturation ratios of n-propanol vapor on tungsten oxide and silver seed particles, respectively. Open circles (red) represent neutral seed particles, while all other data were obtained with positively charged seed particles. Colors blue and red refer to expansion chamber temperatures of 15°C and 25°C, respectively. Black stars are experimental data reported by Winkler et al. (2008a).

3.2. Onset saturation ratio

Onset saturation ratios S_{onset} of n-propanol vapor on charged and neutral seed particles with diameters ranging from about 1 nm to 10 nm were determined by evaluating experimental heterogeneous nucleation probability curves $P(S_0)$. $P(S_0)$ data are obtained using the total number concentration of particles inside the expansion chamber as reference. Thus, unlike counting efficiencies, $P(S_0)$ is independent of sampling losses. Figure 11 shows the results plotted as a function of geometric seed particle diameter d^g_{seed} (Larriba et al. 2011). Circles and stars represent data for silver and tungsten oxide particles, respectively. Open circles (red) represent neutral seed particles while all other data were obtained with positively charged seed particles. Colors blue and red indicate system temperature settings low and high, respectively. Dashed (red) and dotted (blue) lines were calculated using the Kelvin equation, which gives the diameter of a droplet in equilibrium with the supersaturated ambient vapor. The solid (red) line shows the Fletcher diameter (contact angle 0°).

S_{onset} data for neutral silver particles (open red circles) are in good agreement with the Fletcher curve. Experiments with charged silver particles (solid red circles) result in onset saturation ratios lower than those predicted by the Fletcher theory. This effect can be explained qualitatively by the lowering of free energy barrier in the presence of charged seed particles, that is, ion induced nucleation (Thomson 1906). Tungsten oxide data determined with vSANC (open blue stars) agree with SANC data (solid black stars, Winkler et al. 2008a) within measurement uncertainties. However onset saturation ratios determined with vSANC have weaker size dependence in agreement with theoretical predictions of Fernandez de la Mora (2011). Further experiments and data analysis are planned to investigate this effect.

Both the agreement between experiment and theory for neutral seeds as well as the agreement between vSANC and SANC data indicate the proper performance of vSANC.

3.3. Field deployment

Field measurements with the vSANC were conducted in spring 2014 at the boreal forest ecosystem measurement station SMEAR II (Station for Measuring Ecosystem-Atmosphere Relations; Hari and Kulmala 2005; Dal Maso et al. 2005).

Atmospheric NPF could be observed with the vSANC only when operating temperatures (T_{sat} = 13°C/T_i = 15°C) were close to the ambient air temperature (5°C–15°C, $RH(15°C) \approx 20\%$). At higher operating temperatures (23°C/25°C) no NPF event was measured indicating that particle evaporation occurred along the inlet line, causing substantial counting losses.

The polydisperse nature of atmospheric samples in combination with a relatively high intake flow rate

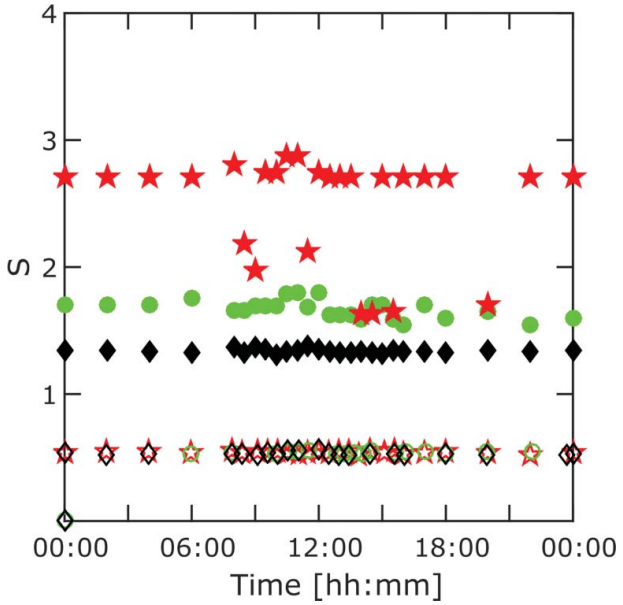

Figure 12. N-propanol saturation ratios S before (open symbols) and after (solid symbols) expansion during field measurements (23 April 2014, $T_{amb} \approx (5^{\circ}C - 15^{\circ}C)$, $\mathrm{RH}_{amb}(15^{\circ}C) \approx 20\%$).

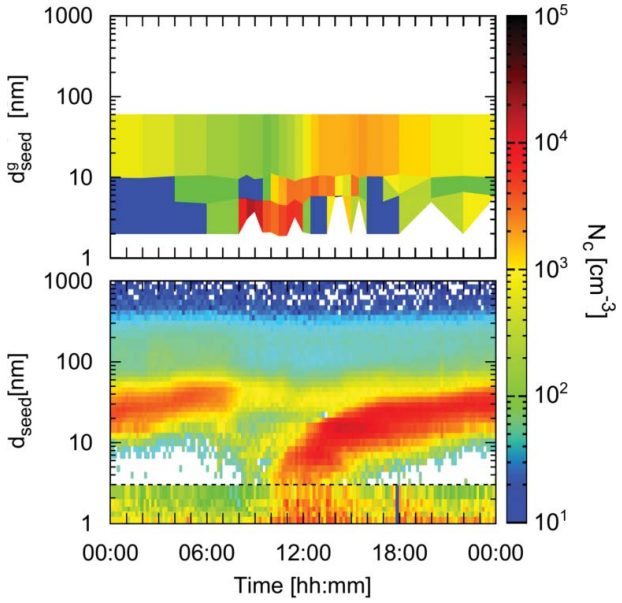

Figure 13. vSANC (top), DMPS (bottom, 3–1000 nm), and nCNC (bottom, 1–3 nm) contour plots from 23 April 2014.

(9 l/min) yielded heterogeneous nucleation and droplet growth to start before the end of expansion, particularly at the highest expansion ratio. This, in turn, resulted in fluctuating S_0. From Figure 12, it can be seen, that despite stable initial vapor saturation ratios S_i of about 0.52 (open symbols) vapor supersaturations S_0 at the end of expansion fluctuate. Strongest fluctuations occur at highest expansion ratios (solid red stars). As a result size bin margins varied with time, which was taken into account by rigorous analysis of experimental Mie curves. Averaged size bin margins for this particular measurement day are listed in Table 1.

Diurnal concentration evolution during atmospheric NPF events show that particle concentrations as high as $10^4 \mathrm{cm}^{-3}$ were detected in the smallest size bin (2–5 nm) about 2–3 h before the NPF signal appeared in a differential mobility particle sizer (DMPS; Aalto et al. 2001; Figure 13). Note that the DMPS charges particles prior to mobility classification, whereas vSANC sizes also neutral particles. Varying margins of the lowest vSANC size bin result from varying S_0 (Figure 12). Simultaneous measurements with the nCNC operated in scanning mode, giving a size distribution between about 1 and 3 nm (Lehtipalo et al. 2014), showed an increase in the concentration of sub-3 nm clusters starting around 8 AM local time in agreement with vSANC data.

On May 3, no particles below 4 nm in diameter have been detected by vSANC, which is in good agreement with DMPS data (Figure 14). The cluster concentrations detected by the nCNC varied throughout the day, but did not indicate clear growth starting from the cluster band to larger sizes.

Unlike the nCNC, vSANC could not observe a continuously present pool of sub-2 nm particles, as suggested

Table 1. Averaged vSANC size bin margins for 23 April 2014.

Size Bin	$d_{\mathrm{seed}}^{g,min}$ [nm]	$d_{\mathrm{seed}}^{g,max}$ [nm]
1	10.1 ± 1.4	–
2	5.4 ± 0.4	10.1 ± 1.4
3	2.3 ± 0.5	5.4 ± 0.4

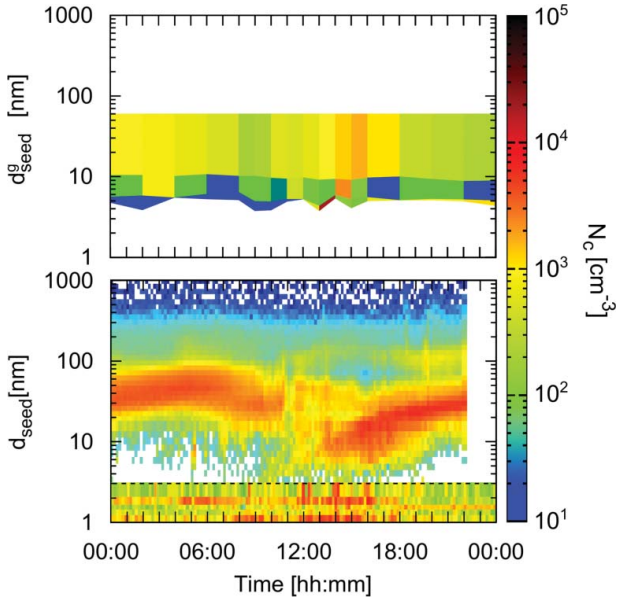

Figure 14. vSANC (top), DMPS (bottom, 3–1000 nm), and nCNC (bottom, 1–3 nm) contour plots from 3 May 2014.

by Kulmala et al. (2007). The discrepancy between the nCNC and vSANC data can possibly be explained by higher inlet losses and insufficient saturation of the latter. This might yield signals resulting from 1 to 2 nm particles being superimposed by signals of larger particles, which are activated earlier in time. It is, therefore, planned to improve vSANC's inlet system, particularly its saturation unit.

During zero measurements binary homogeneous nucleation of water and n-propanol was observed in the expansion chamber at high ambient relative humidity (RH). An all-campaign average of experimental Mie curves from homogeneous nucleation tests is shown in Figure 15. Dash-dotted (blue), dashed, and solid (green) lines refer to approximately 90, 45, and 25% ambient RH at 15°C, respectively. It can be clearly seen, that as ambient RH increases homogeneous nucleation starts at lower pressure drops. This is a strong indicator for binary nucleation of n-propanol and water. Fortunately, NPF events usually occurred at sufficiently low RH. Thus binary nucleation could be neglected in data analysis.

4. Summary

A novel expansion-type CPC—the versatile Size Analyzing Nuclei Counter (vSANC)—its performance and application to ambient aerosol studies are presented.

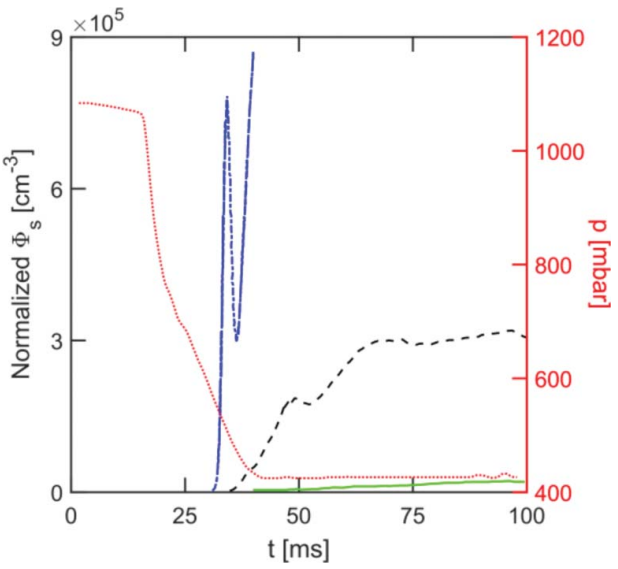

Figure 15. Influence of RH on the onset of homogeneous nucleation inside the particle free expansion chamber at constant expansion ratio. Dash-dotted (blue), dashed, and solid (green) lines represent all-campaign averages of normalized experimental 15° Mie curves measured at about 90, 45, and 25% ambient RH. Heights of first Mie maxima correspond to about 7.8×10^5 cm^{-3}, 1.8×10^5 cm^{-3}, and $<10^3$ cm^{-3} homogeneously formed droplets at 90, 45, and 25% ambient RH, respectively. The dotted (red) line shows the chamber pressure.

The operation of the vSANC is based on heterogeneous nucleation of supersaturated vapor on preexisting aerosol particles and subsequent droplet growth. Well-defined uniform vapor supersaturation inside the expansion chamber is achieved by adiabatic expansion. Nanoparticles activated by heterogeneous nucleation are grown to larger sizes and can be detected by light scattering. The measuring principle was adopted from the classical SANC (Wagner 1982; Wagner et al. 2003).

The vSANC was designed to allow maximum flexibility for its application in field as well as laboratory studies. This includes wide ranges of operating temperatures and total gas pressures, −20°C to +40°C and 0.2 to 1.2 bar, respectively, and flexibility with respect to the choice of condensing liquids and aerosol intake flow rates.

Counting efficiency measurements show that vSANC detects 10–20% of particles/clusters at 1.5 nm in diameter, the 50% cut-off size being about 4.3 nm. Thus, it can be used as particle counter for sub-3 nm clusters. Particle number concentrations and growth curves are obtained by means of an optical detection technique–the multiangle Constant Angle Mie Scattering method (mCAMS). This way we can precisely measure the evolution of droplet size as a function of time (Wagner 1985). Simultaneous measurement of the transmitted light flux allows to determine absolute droplet number concentrations (Szymanski and Wagner 1990) ranging from 10^2 to 10^7 cm^{-3}. Droplet growth data enable precision determination of vapor saturation ratios, which are the key in evaluating sizes of molecular clusters down to about 1 nm using heterogeneous nucleation probability curves (Winkler et al. 2012).

In spring 2014, the vSANC was operated at the SMEAR II station in Hyytiälä, Finland. The main goal was to investigate the formation and growth of atmospheric clusters starting from smallest detectable sizes. To this end, the vSANC was operated in scanning mode, where size-dependent particle activation is achieved by altering the expansion ratio among three different values. Accordingly, size-resolved concentration measurements in the particle diameter bins 2–5 nm, 5–10 nm, and > 10 nm were performed sequentially, one full measuring sequence taking about six minutes. At the highest pressure drop close to the onset of homogeneous nucleation basically all clusters capable of acting as condensation nuclei can be considered activated. Using n-propanol as working fluid, atmospheric NPF could be observed only when operating temperatures were close to the ambient air temperature.

Diurnal concentration evolution during atmospheric NPF events showed that particle concentrations as high as 10^4 cm^{-3} were detected in the smallest size bin

(2–5 nm) about 2–3 h before the NPF signal appeared in a DMPS. A continuously present pool of highly concentrated neutral clusters in the sub-3 nm size range Kulmala et al. (2007) could not be confirmed during these measurements. This is mainly related to the fact that our smallest size bin is 2–5 nm whereas the expected pool is typically in the sub-2 nm size range (see Kulmala et al. 2013). Ongoing work on vSANC inlet design and optimization of the saturation system aim at reducing the lower size cut-off considerably.

Acknowledgments

The valuable contributions by A. Glaser and O. Gabriel to design and construction of the vSANC are gratefully acknowledged. The authors thank the reviewers for their detailed comments, which have led to several improvements of the manuscript.

Funding

The research leading to these results has received funding from the European Research Council under the European Community's Seventh Framework Programme (FP7/2007-2013)/ERC grant agreement No. 616075 (NANODYNAMITE) and No. 262254 (ACTRIS), the European Union's Horizon 2020 research and innovation program under the Marie Sklodowska-Curie programme (grant no. 656994) from the Top-level Research Initiative (Cryosphere-atmosphere interactions in a changing Arctic climate—CRAICC) and from the Austrian Science Fund (P19546, L593).

References

Aalto, P., Hämeri, K., Becker, E., Weber, R., Salm, J., Mäkelä, J. M., and Kulmala, M. (2001). Physical Characterization of Aerosol Particles During Nucleation Events. *Tellus*, 53 (B):344–358.

Andreae, M. O. (2013). The Aerosol Nucleation Puzzle. *Science*, 339(6122):911–912.

Dal Maso, M., Kulmala, M., Riipinen, I., Wagner, R., Hussein, T., Aalto, P., and Lehtinen, K. (2005). Formation and Growth of Fresh Atmospheric Aerosols: Eight Years of Aerosol Size Distribution Data from SMEAR II, Hyytiälä, Finland. *Boreal Environ. Res.*, 10:323–336.

Fernandez de la Mora, J. (2011). Heterogeneous Nucleation with Finite Activation Energy and Perfect Wetting: Capillary Theory versus Experiments with Nanometer Particles, and Extrapolations on the Smallest Detectable Nucleus. *Aerosol. Sci. Tech.*, 45(4):543–554.

Fletcher, N. (1958). Size Effect in Heterogeneous Nucleation. *J. Chem. Phys.*, 29:572–576.

Gamero-Castaño, M., and Fernandez de la Mora, J. (2002). Ion-Induced Nucleation: Measurement of the Effect of Embryo's Size and Charge State on the Critical Supersaturation. *J. Chem. Phys.*, 117:3345.

Gamero-Castaño, M., and Fernández de la Mora, J. (2000). A Condensation Nucleus Counter (CNC) Sensitive to Single Charged Sub-Nanometer Particles. *J. Aerosol. Sci.*, 31:757–772.

Hari, P., and Kulmala, M. (2005). Station for Measuring Ecosystem-Atmophere Relations (SMEAR II). *Boreal Environ. Res.*, 10, 351–322.

Hering, S. V., Stolzenburg, M. R. S., Quant, F. R., Oberreit, D. R., and Keady, P. B. (2005). A Laminar Flow Water Based Condensation Particle Counter WCPC. *Aerosol. Sci. Tech.*, 39(7):659–672.

Iida, K., Stolzenburg, M. R., and McMurry, P. H. (2009). Effect of Working Fluid on Sub-2 nm Particle Detection with a Laminar Flow Ultrafine Condensation Particle Counter. *Aerosol. Sci. Tech.*, 43(1):81–96.

Kalivitis, N., Kerminen, V.-M., Kouvarakis, G., Stavroulas, I., Bougiatioti, A., Nenes, A., and Mihalopoulos, N. (2015). Atmospheric New Particle Formation as a Source of CCN in the Eastern Mediterranean Marine Boundary Layer. *Atmos. Chem. Phys.*, 15(16), 9203–9215.

Kangasluoma, J., Attoui, M., Korhonen, F., Ahonen, L., Siivola, E., and Petäjä, T. (2016). Characterization of a Herrmann Type High Resolution Differential Mobility Analyzer. *Aerosol. Sci. Tech.*, 50(3):222–229.

Kangasluoma, J., Junninen, H., Lehtipalo, K., Mikkilä, J., Vanhanen, J., Attoui, M., and Petäjä, T. (2013). Remarks on Ion Generation for CPC Detection Efficiency Studies in Sub-3-nm Size Range. *Aerosol. Sci. Tech.*, 47(5):556–563.

Kuang, C. A., Chen, M. D., McMurry, P. H., and Wang, J. (2012). Modification of Laminar Flow Ultrafine Condensation Particle Counters for the Enhanced Detection of 1 nm Condensation Nuclei. *Aerosol. Sci. Tech.*, 46 (3):309–315.

Kulmala, M., Kontkanen, J., Junninen, H., Lehtipalo, K., Manninen, H. E., Nieminen, T., and Worsnop, D. R. (2013). Direct Observations of Atmospheric Aerosol Nucleation. *Science*, 339(6122), 943–946.

Kulmala, M., Riipinen, I., Sipilä, M., Manninen, H. E., Petäjä, T., Junninen, H., and Kerminen, V.-M. (2007). Toward Direct Measurement of Atmospheric Nucleation. *Science*, 318(5847):89–92.

Kulmala, M., Vehkamäki, H., Petäjä, T., Dal Maso, M., Lauri, A., Kerminen, V. M., and McMurry, P. H. (2004). Formation and Growth Rates of Ultrafine Atmospheric Particles: A Review of Observations. *J. Aerosol. Sci.*, 35(2):143–176.

Kupc, A., Winkler, P. M., Vrtala, A., and Wagner, P. E. (2013). Unusual Temperature Dependence of Heterogeneous Nucleation of Water Vapor on Ag Particles. *Aerosol. Sci. Tech.*, 47(9):i–iv.

Larriba, C., Hogan, C. J., Attoui, M., Borrajo, R., Garcia, J. F., and de la Mora, J. F. (2011). The Mobility–Volume Relationship below 3.0 nm Examined by Tandem Mobility–Mass Measurement. *Aerosol. Sci. Tech.*, 45(4):453–467.

Lehtipalo, K., Leppä, J., Kontkanen, J., Kangasluoma, J., Franchini, A., Wimmer, D., and Kulmala, M. (2014). Methods for Determining Particle Size Distribution and Growth Rates Between 1 and 3 nm using the Particle Size Magnifier. *Boreal Environ. Res.*, 19(B), 15–236.

Liu, B. Y. H., and Kim, C. S. (1977). On the Counting Efficiency of Condensation Nuclei Counters. *Atmos. Environ.*, 11:1097.

McMurry, P. H. (2000a). A Review of Atmospheric Aerosol Measurements. *Atmos. Environ.*, 34(12–14):1959–1999.

McMurry, P. H. (2000b). The History of Condensation Nucleus Counters. *Aerosol. Sci. Tech.*, 33(4):297–322.

Merikanto, J., Spracklen, D. V., Mann, G. W., Pickering, S. J., and Carslaw, K. S. (2009). Impact of Nucleation on Global CCN. *Atmos. Chem.Phys. Discuss.*, 9, 8601–8616.

Okuyama, K., Kousaka, Y., and Motouchi, T. (1984). Condensational Growth of Ultrafine Aerosol Particles in a New Particle Size Magnifier. *Aerosol. Sci. Tech.*, 3(4):353–366.

Petäjä, T., O'Connor, E. J., Moisseev, D., Sinclair, V. A., Manninen, A. J., Väänänen, R., and Hickmon, N. (2016). BAECC A Field Campaign to Elucidate the Impact of Biogenic Aerosols on Clouds and Climate. *Bull. Am. Meteorol. Soc.*, accepted. http://doi.org/10.1175/BAMS-D-14-00199.1

Reischl, G. P., Mäkelä, J., and Necid, J. (1997). Performance of Vienna Type Differential Mobility Analyzer at 1.2–20 Nanometer. *Aerosol. Sci. Tech.*, 27:651–672.

Reischl, G. P., Scheibel, H. G., and Porstendörfer, J. (1983). The Bipolar Charging of Aerosols. *Colloid. Int. Sci.*, 91(1):272–275.

Richarz, F. (1906). Der Wert des Verhältnisses der beiden spezifischen Wärmen für ein Gemisch zweier Gase, insbesondere für ozonhaltigen Sauerstoff. *Ann. Phys.*, 19:639.

Scheibel, H. G., and Porstendörfer, J. (1983). Generation of Monodisperse Ag- and NaCl-aerosols with Particle Diameters Between 2 and 300 nm. *J. Aerosol. Sci.*, 14(2):113–126.

Schobesberger, S., Winkler, P. M., Pinterich, T., Vrtala, A., Kulmala, M., and Wagner, P. E. (2010). Experiments on the Temperature Dependence of Heterogeneous Nucleation on Nanometer-sized NaCl and Ag Particles. *ChemPhysChem*, 11(18):3874–3882.

Seto, T., Okuyama, K., and Fernández de la Mora, J. (1997). Condensation of Supersaturated Vapors on Monovalent and Divalent Ions of Varying Size. *J. Chem. Phys.*, 107:1576–1585.

Sihto, S. L., Mikkilä, J., Vanhanen, J., Ehn, M., Liao, L., Lehtipalo, K., and Kulmala, M. (2011). Seasonal Variation of CCN Concentrations and Aerosol Activation Properties in Boreal Forest. *Atmos. Chem. Phys.*, 11(24):13269–13285.

Sipilä, M., Lehtipalo, K., Attoui, M., Neitola, K., Petäjä, T., Aalto, P. P., and Kulmala, M. (2009). Laboratory Verification of PH-CPC's Ability to Monitor Atmospheric Sub-3 nm Clusters. *Aerosol. Sci. Tech.*, 43(2):126–135.

Sipilä, M., Lehtipalo, K., Kulmala, M., Petäjä, T., Junninen, H., Aalto, P. P., and O'Dowd, C. D. (2008). and Physics Applicability of Condensation Particle Counters to Measure Atmospheric Clusters. *Atmos. Chem. Phys.*, 8:4049–4060.

Spracklen, D. V., Carslaw, K. S., Kulmala, M., Kerminen, V. M., Sihto, S. L., Riipinen, I., and Lihavainen, H. (2008). Contribution of Particle Formation to Global Cloud Condensation Nuclei Concentrations. *Geophys. Res. Lett.*, 35 (6):1–5.

Steiner, G. (2006). *Generation of Nanoparticles - about the Construction of a Heating Wire Tungsten Oxide Particle Generator*. University of Vienna, Vienna, Austria.

Stolzenburg, M. R., and McMurry, P. H. (1991). An Ultrafine Aerosol Condensation Nucleus Counter. *Aerosol. Sci. Tech.*, 14:48–65.

Szymanski, W. W., and Wagner, P. E. (1990). Absolute Aerosol Number Concentration Measurement by Simultaneous Observation of Extinction and Scattered Light. *J. Aerosol. Sci.*, 21:441–451.

Thomson, J. J. (1906). *Conduction of Electricity Through Gases*. Cambridge University Press, Cambridge, UK.

Vanhanen, J., Mikkilä, J., Lehtipalo, K., Sipilä, M., Manninen, H. E., and Siivola, E. (2011). Particle Size Magnifier for Nano-CN Detection. *Aerosol. Sci. Tech.*, 45:533–542.

Vehkamäki, H., Määttänen, A., Lauri, A., Kulmala, M., Winkler, P., Vrtala, A., and Wagner, P. E. (2007). Heterogeneous Multicomponent Nucleation Theorems for the Analysis of Nanoclusters. *J. Chem. Phys.*, 126(17):174707-1–174707-12.

Vesala, T., Kulmala, M., Rudolf, R., Vrtala, A., and Wagner, P. E. (1997). Models for Condensational Growth and Evaporation of Binary Aerosol Particles. *J. Aerosol. Sci.*, 24:565–598.

Wagner, P. E. (1982). *Aerosol Microphysics II*. Springer: Berlin, Heidelberg, New York. p. 129.

Wagner, P. E. (1985). A Constant-Angle Mie Scattering Method (CAMS) for Investigation of Particle Formation Processes. *J. Colloid Interf. Sci.*, 105:456–467.

Wagner, P. E., Petersen, D., Vrtala, A., Lauri, A., Kulmala, M., and Laaksonen, A. (2003). Nucleation Probability in Binary Heterogeneous Nucleation of Water - n-Propanol Vapor Mixtures on Insoluble and Soluble Nanoparticles. *Phys. Rev. E*, 67:021605–1.

Winkler, P. M., Steiner, G., Vrtala, A., Vehkamäki, H., Noppel, M., Lehtinen, K., and Kulmala, M. (2008a). Heterogeneous Nucleation Experiments Bridging the Scale from Molecular Ion Clusters to Nanoparticles. *Science*, 319(5868):1374–1377.

Winkler, P. M., Vrtala, A., and Wagner, P. E. (2008b). Condensation Particle Counting Below 2 nm Seed Particle Diameter and the Transition from Heterogeneous to Homogeneous Nucleation. *Atmos. Res.*, 90(2–4):125–131.

Winkler, P. M., Vrtala, A., Steiner, G., Wimmer, D., Vehkamki, H., Lehtinen, K. E. J., and Wagner, P. E. (2012). Quantitative Characterization of Critical Nanoclusters Nucleated on Large Single Molecules. *Phys. Rev. Lett.*, 108(8):1–5.